Eur. Phys. J. Special Topics **223**, 2285–2295 (2014)
© EDP Sciences, Springer-Verlag 2014
DOI: 10.1140/epjst/e2014-02264-1

THE EUROPEAN PHYSICAL JOURNAL SPECIAL TOPICS

Review

A soft matter in construction – Statistical physics approach to formation and mechanics of C–S–H gels in cement

E. Del Gado[1,2,a], K. Ioannidou[3,7], E. Masoero[4], A. Baronnet[5], R.J.-M. Pellenq[3,5,7], F.-J. Ulm[3,7], and S. Yip[6]

[1] Department of Physics and Institute for Soft Matter Synthesis & Metrology, Georgetown University, Washington DC, USA
[2] Department of Civil, Environmental and Geomatic Engineering, ETH Zurich, Zurich, Switzerland
[3] Department of Civil and Environmental Engineering, Massachusetts Institute of Technology, Cambridge, USA
[4] School of Civil Engineering and Geosciences, Newcastle University, Newcastle upon Tyne, UK
[5] CINaM, CNRS and Aix-Marseille University, Marseille, France
[6] Department of Nuclear Science and Engineering, Massachusetts Institute of Technology, Cambridge, USA
[7] <MSE>^{2}, MIT-CNRS Joint Laboratory, Massachusetts Institute of Technology, Cambridge, USA

Received 4 June 2014 / Received in final form 18 August 2014
Published online 24 October 2014

Abstract. Calcium-silicate hydrate (C–S–H) is the main binding agent in cement and concrete. It forms at the beginning of cement hydration, it progressively densifies as cement hardens and is ultimately responsible of concrete performances. This hydration product is a cohesive nano-scale gel, whose structure and mechanics are still poorly understood, in spite of its practical importance. Here we review some of the open questions for this fascinating material and a statistical physics approach recently developed, which allows us to investigate the gel formation under the out-of-equilibrium conditions typical of cement hydration and the role of the nano-scale structure in C–S–H mechanics upon hardening. Our approach unveils how some distinctive features of the kinetics of cement hydration can be related to changes in the morphology of the gels and elucidates the role of nano-scale mechanical heterogeneities in the hardened C–S–H.

1 Introduction

Cement dissolves in contact with water and a number of different hydration products precipitate from the ionic pore solution. In particular, the development of an inorganic cohesive hydrogel, the calcium-sylicate-hydrate (C–S–H), is at the core of cement main

[a] e-mail: ed610@georgetown.edu

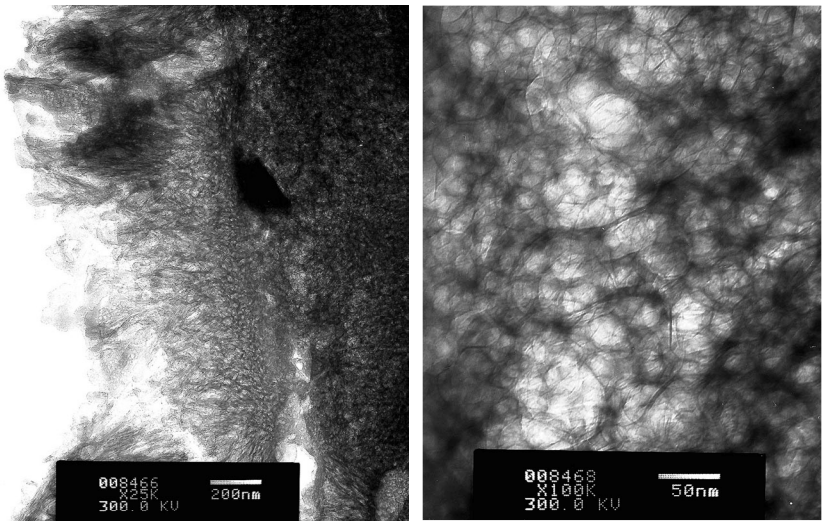

Fig. 1. Bright-field TEM images of C–S–H gels. Left: two standard textures of the gel: low-density and fibrous on the left side, high-density, more isotropic on the right side. Right: blown-up TEM image of high-density C–S–H showing thin crystalline platelets surrounding nanopores.

function as the binding agent in concrete for buildings and infrastructures. Strength and several aspects of concrete mechanics depend on the nano-scale features of this complex and still quite mysterious gel [1]. Moreover, the CO_2 associated to cement production, mainly due to burning limestone and various minerals in high temperature kilns, amounts to 5–8% of the global human CO_2 production, because of the huge volume used. Hence, not only improving and designing the material performances, but also reducing its environmental footprint challenge the current understanding of the fundamental physico-chemical mechanisms involved in the development of C–S–H morphology and mechanics [2,3].

The C–S–H gel progressively assembles and densifies during cement hydration, glueing together the final solid product [4–7]. In the early stages of the hydration, the gel rapidly fills the pore space, growing over a few hundreds of nanometers. Experimental observations, mainly performed after setting, reveal a disordered and heterogeneous texture. Figure 1 shows TEM images of C–S–H gels obtained during hydration of tricalcium silicate – C3S (the main source of C–S–H in Portland cement and often used as a model system for cement hydration). The left image displays the coexistence of high- and low-density gels along a sharp interface. This boundary marks the outline of a resorbed C3S grain (on the right side) which reacted to, and was mostly replaced inside by, nanoporous high-density C–S–H (HD-C–S–H). Excess C3S solute exported across the boundary insured supersaturation of the surrounding aqueous solution with respect to C–S–H so that low-density, fibrous, C–S–H (LD-C–S–H) crystallized in the free space of solution outside this boundary. A highly porous nanotexture of the pseudomorphic HD C–S–H is shown in the image on the right, where C–S–H platelets, a few tens of nanometers in width and a few nanometers thick, are connected mainly edgewise around pores. One has to recognise that external conditions during hydration may significantly affect C–S–H growth and morphology. Nevertheless, the layered or fibrillar texture in the amorphous C–S–H gel as well as the presence of structural units (platelets) with a typical size of the order of 10 nm are quite robust features. They are supported by neutron scattering and AFM experiments [5,8–10]. The typical size 1–30 nm of the colloidal nano-scale C–S–H

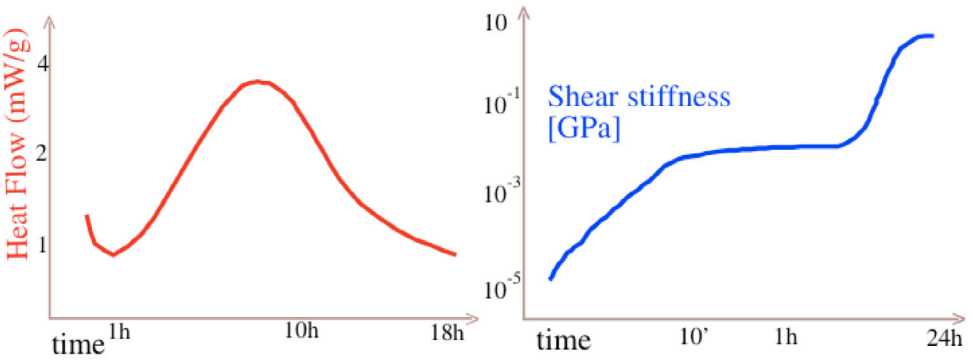

Fig. 2. Left: schematics of the time dependence of the heat flow during hydration, typically obtained in calorimetry measurements. Right: schematics of the shear stiffness as a function of time in a cement paste during hydration and setting.

platelets and an internal layered structure [4,5,8,10–12] gives a good indication of the typical size of locally compact calcium-silicate layers [1].

The chemical and physical environment changes as the hydration proceeds and provides quite unique out-of-equilibrium conditions for the gel growth: the heat flow associated to C–S–H formation and measured via calorimetry has a non-monotonic dependence on time, with a hallmark peak separating an acceleration and a deceleration regime in the hydration kinetics [11,13]. Several indirect observations suggest that such features must be related to changes in the gel morphology (and mechanics), but a coherent microscopic picture is still missing. Figures 2 shows the schematics of the time dependence of the heat flow measured via calorimetry during cement hydration (left) and of the shear stiffness during cement hydration and setting (right), which has been measured via rheology or ultrasound spectroscopy [14,15]: the transition from the accelerated to the decelerating kinetics roughly coincides with the final dramatic increase of the shear stiffness that leads to the cement setting.

The early-stages of the hydration, when the gel is still relatively soft, are particularly important because they offer a unique possibility to control/modify the material properties at the nanometer scale or at the level of the basic chemical components, which is far from trivial in a material of such complexity. Nevertheless, how changing chemical components and/or modifying the hydration conditions affect the development of the C–S–H gels is far from being well understood. This is becoming a compelling question to be addressed, since the forefront of research in cement is in more sustainable chemical modifications that would allow to reduce the CO_2 footprint of the material. Recent nano-scale experiments support the general understanding that the meso-scale structure of C–S–H impacts macro-scale properties [16,17]. Hence identifying the physico-chemical origin of such properties of C–S–H could lead to a real breakthrough into how to design new *green* formulations of cement without sacrificing the mechanical performance.

The range of length-scales from several tens to hundreds of nanometers, typical of soft matter systems, is particularly crucial for C–S–H. The structural heterogeneity and lack of long-range order that arise over these length-scales have clearly a role in its mechanical response [17]. This range of length-scales has been hardly addressed by modeling and computational studies that, so far, have been mostly focused on sub-nanometer scales or, to the other end, on the micron-scale structure of the C–S–H phase [18–20]. In this paper, we give a brief overview of recent results obtained specifically for this range of length scales via statistical mechanics models and numerical simulations. We discuss new ideas for investigating the formation of the gel under

out-of-equilibrium conditions of the type associated to cement hydration and for unraveling the nano-scale origin of the mechanical properties of C–S–H in the hardened paste. The results obtained demonstrate that novel, significant insight into the material properties can be gained, opening the way towards obtaining a quantitative, physically grounded microscopic picture of cement.

The paper is organized as follows. In Sect. 2, we review the approach recently proposed for investigating the hydration kinetics and the formation of C–S–H gels during the early ages of cement hydration [31]. We use the results of the numerical simulations to gain new understanding of the possible connections between the changes in the gel morphology and the different stages of the hydration process. A direct connection with experimental observations is attempted and the relevance to different qualitative scenarios suggested in the literature is discussed. In Sect. 3, we focus on the later stages of cement hydration, where C–S–H gels are highly dense and cohesive. Through numerical simulations of a polydisperse colloidal model, we show that the indentation modulus of C–S–H measured in experiments can be understood in terms of significant nano-scale mechanical heterogeneities.

2 Hydration kinetics and gel morphology

A few aspects of the growth of C–S–H gels during cement hydration can be rationalised in terms of irreversible aggregation models [21], in particular along the line of DLA or DLCA of the colloidal units [5,22,23]. Nevertheless, there is little evidence of a fractal aggregation nor the final gel morphology can be easily related to this type of process [24,25]. Moreover, a fractal type of growth cannot be immediately related to the features of the hydration kinetics shown in Fig. 2 (left). A growth mechanism based on sheets or ribbons of crystalline C–S–H that would branch because of the defects produced during precipitation, has been proposed as an alternative to the fractal aggregation of nanoparticles [26,27]. Although the idea has never been translated into an analytical or computational approach to quantitatively test it, it does capture many features of the final gel morphology (as shown for example in SEM images [25] or indicated by NMR studies [28]), in addition to being consistent with the hydration kinetics: the acceleration can be related to the nucleation and growth of the elongated structures (that are crystalline or semicrystalline), whose steric interactions, impingement or branching would eventually determine the deceleration regime and the final mesoscale amorphous organization of the gel [29,30].

We have recently proposed a new approach where, without imposing a specific growth mechanism for the gel, the aggregation of the C–S–H hydrates and their assembly into a gel naturally emerge from the thermodynamics of the hydrates in solution and the out-of-equilibrium condition imposed by the chemical environment typical of cement hydration [31]. We focused on a small volume contained in a capillary pore of the wet paste (as suggested, for example, in [32,33]) and approximated it to an open system of interacting colloidal particles. The colloidal particles in the model can be thought of as the C–S–H colloidal units or simply as coarse-grained elements in our description of the material. In a first approximation, we consider such particles to be spherical and monodisperse in size. Size polydispersity and shape anisotropy are certainly important in a material like C–S–H and will be included in the model in future work. Because of the gelation and of the strong cohesion that C–S–H develops, it is clear that the net particle interactions must be attractive. Strong non-contact attractive forces, more than one order of magnitude stronger than Van der Waals interactions, are expected indeed in the presence of high surface charges and of divalent counter-ions Ca^{2+} in the pore solution [1,34–37]. Experiments, simulations and theory also indicate that a narrow and deep attractive interaction well can be

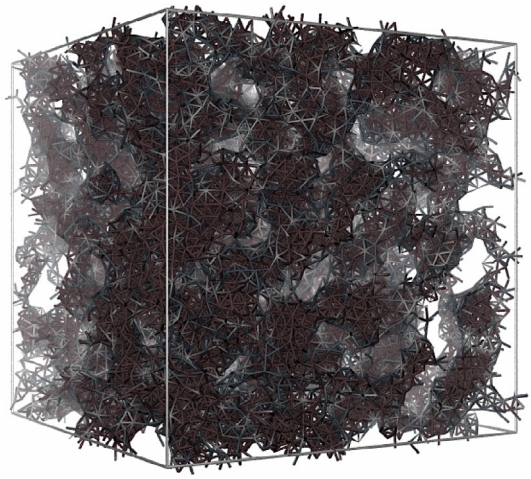

Fig. 3. A snapshot of the gel obtained in the simulations of our model for the formation of C–S–H gels during cement hydration (the data are from Ref. [31]).

accompanied by a medium range repulsive shoulder [35,38–41], whose strength is mainly determined by the lime concentration [10], which in general changes with time during cement hydration, hence changing the effective interparticle potential over time. Using the experimental measurements of Ref. [38] as guideline, we have included this information in the interaction potential between the colloidal particles in Molecular Dynamics (MD) simulations of our model hydrate suspension and studied different cases corresponding to different lime concentrations (and hence different stages of the hydration process), as discussed in detail in Ref. [31].

The assembly of C–S–H gels during cement hydration is quite different from most gelation processes investigated in other soft matter systems because of the underlying hydration kinetics that produces the material as gelation proceeds. We have included these specific out-of-equilibrium conditions for gelation by coupling the MD simulations with a Grand-canonical Monte Carlo scheme (GCMC) that mimics the precipitation of C–S–H, with the chemical potential representing the free energy gain corresponding to the formation of the C–S–H hydrates (i.e., its value sets the equilibrium density of C–S–H that can be reached in the pore). The number of GCMC attempts N_{MC} over the number of MD steps N_{MD} defines the rate $R = N_{MC}/N_{MD}$, i.e., the rate of producing hydrates which is determined by the chemical environment. By varying R, we can investigate how the gelation process may change due to a fast/slow precipitation of C–S–H. A full account and details of the simulations can be found in Ref. [31]. Here, we would like to focus on a few specific results and on the new insight that they allowed us to gain.

Figure 3 shows a snapshot of the gel formed in the simulations just described: one can recognize that the mesoscale organization of the gel is disordered and characterized by large pores, in spite of the fact that, more locally, particles can be quite densely packed, with a certain degree of local order and anisotropy. This type of gel structure is quite common when short range attractive interactions compete with a medium range repulsion and results from the interplay between the thermodynamics that tend to favor large and anisotropic self-assembled structures such as fibrils and lamellae and the emergence of gelation [42,43]. This combination of a certain degree of local order and anisotropy with long range disorder is consistent with several observations in C–S–H gels [25,28,44]. Varying the rate R in the simulations proves that varying the chemical environment changes the out-of-equilibrium conditions under

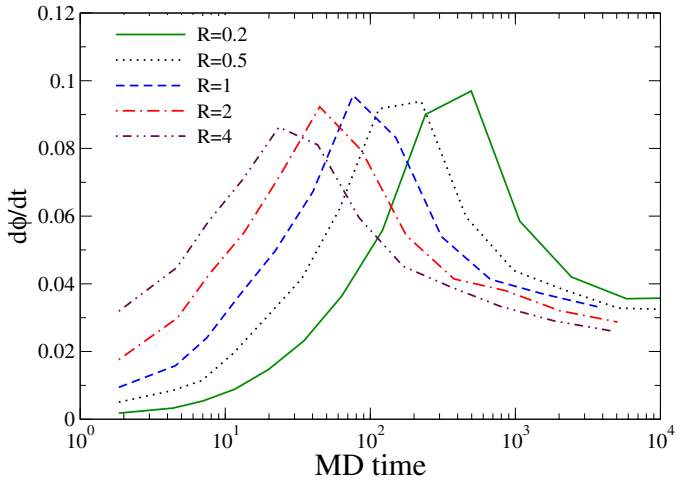

Fig. 4. The rate of hydration, computed as $\dot{\phi}(t)$ in the simulations of the model described in Sect. 2, plotted as a function of time for different precipitation rates R (the data are from Ref. [31]). The data display a peak separating the accelerating and the decelerating regimes of the hydration kinetics, similar to the hallmark of cement hydration.

which the C–S–H gel develops and may significantly affect the development of the gel morphology. The fraction $\phi(t)$ of the volume of the simulation box that is progressively occupied by C–S–H can be related to the degree of hydration and the rate at which it changes, $\dot{\phi}(t)$, to the hydration rate measured in calorimetry experiments (Fig. 2, left). In Fig. 4, we plot $\dot{\phi}(t)$ as a function of the MD time: the non-monotonic behavior is strongly reminiscent of the one typical of cement hydration, with the peak allowing us to clearly identify the accelerating and decelerating regimes of the kinetics. The time evolution of the $\phi(t)$ obtained from the same simulations is plotted in Fig. 5, displaying indeed the same type of sigmoidal curve typically obtained for the degree of the hydration in experiments [10]. We attempt a comparison with the experimental measurements performed on macroscopic samples, by considering that each Monte Carlo cycle, performed over the duration of the MD simulation time window, does not correspond to an instantaneous process but indeed to the finite time lapse τ_s needed to produce a certain amount of hydrates. Hence an increment in real time of the experiments dt_r should be compared with an increment $(dt_s/\tau_s)\tau_0$ in the simulation time (width τ_0 the MD unit time). The time lapse τ_s is expected to increase as dissolution and hydration proceed, because the increasing density of ions ρ_i in the pore solution that leads to the increasing amount of hydrates will tend to slow down ion diffusion and hydrate formation. If, for small enough time increments, we assume that $\tau_s \propto \rho_i$ and that ρ_i increases linearly with t_s, we obtain that $dt_r \simeq (dt_s/t_s)\tau_0$ and that the elapsed real time t_r should be compared with the logarithm of the simulation time lapse $t_r \propto \ln t_s$. We have used this argument to rescale the real time in comparing the experimental data to the simulation results in Fig. 5, where the black symbols have been obtained from Ref. [10], confirming the agreement between simulations and experiments. This comparison is obviously meant to be qualitative, because the experimental data refer to macroscopic samples of C_3S, whereas the numerical data refer to C–S–H gel in the range of few hundreds of nanometers. Interestingly enough, once we fix the rescaling factors (i.e., we fix the amount of hydrates in the simulations corresponding to the degree of hydration at time 0 in the experiments) for a fixed lime concentration, we can change the lime concentration (i.e. the parameters used

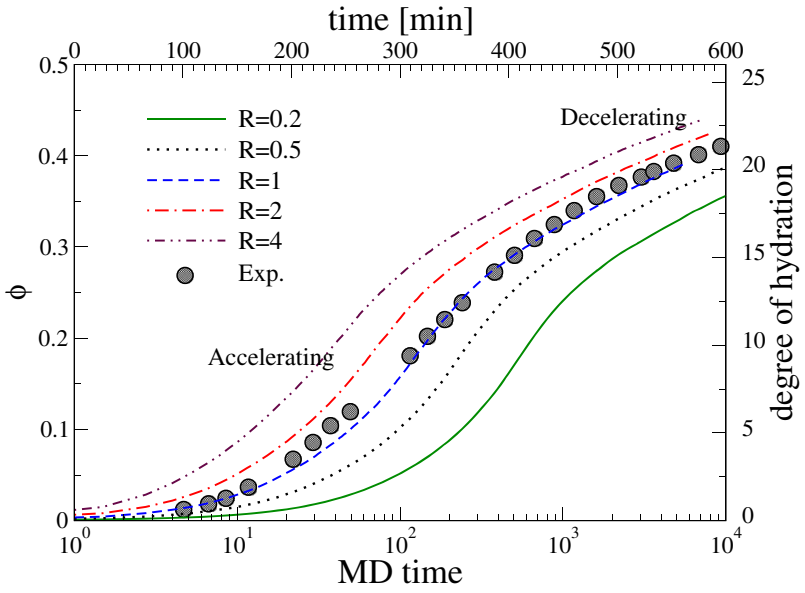

Fig. 5. Evolution of volume fraction ϕ for one of the models described in Sect. 2 over the simulation time, for different precipitation rates R (the data are from Ref. [31]). The black dots are data from experimental measurements of the degree of hydration in Ref. [38] as explained in the text.

in the interaction potential) and recover the same variation of the hydration curve which is displayed by the experimental data [31], i.e., we recover the agreement with the experiments performed in the new conditions. This finding, together with the fact that the changes in the gel morphology detected upon changing the lime concentration in the simulations are consistent with the ones reported in the experiments of Ref. [10], support the idea that our model and approach capture a few fundamental physical mechanisms in the formation of C–S–H gels.

Starting from these encouraging results, we gain some new insight by analyzing the local packing and the gel self-assembly at different stage of the hydration process. At the very early stages, corresponding to a high lime concentration, the acceleration regime of the hydration kinetics can be directly related, in our model, to reaching the optimal local packing that allows for large fibrillar aggregates to grow. This part of the kinetic is clearly controlled by thermodynamics (i.e., it changes qualitatively upon changing the interaction potential and is pretty insensitive to the rate R) whereas the deceleration is controlled by the precipitation rate R: the more chemistry favors hydrate precipitation, the faster the densification and the more dramatic the deceleration. A detailed analysis of the gel morphology shows that, due to the effective interactions between hydrates, the growth of the gel happens via the growth of elongated aggregates that are locally crystalline or semi-crystalline and branch (or impinge) as precipitation proceeds. Such emerging picture is consistent with the model proposed in [26], in spite of the fact that our model is based on colloidal units, reconciling two different views of the material that have been traditionally considered incompatible with each other. Finally, we find evidence that the change in the interaction potential due to the evolving chemical environment during hydration might be key for the further densification of the material, in spite of the decelerating kinetics, by thermodynamically favoring local packing with higher coordination and density.

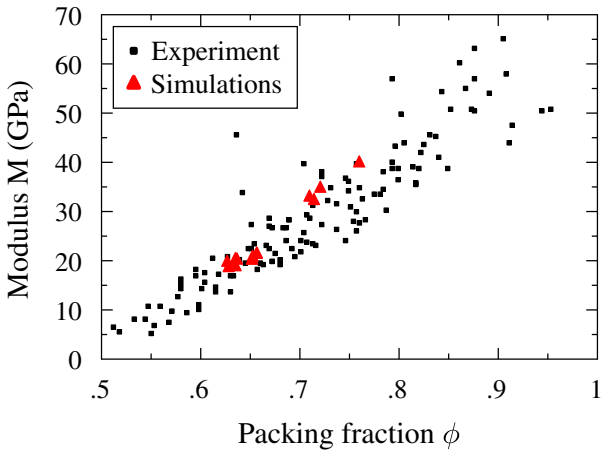

Fig. 6. Indentation moduli vs packing fraction (the data are from Ref. [46]). The data show the comparison between the numerical simulations of the model described in Sect. 3 and nano-indentation experiments [18].

3 Mechanical heterogeneities in the hardened paste

By the end of the hydration process, a dense cohesive C–S–H gel is formed. Nanoindentation has been used to measure the mechanical properties of C–S–H at the sub-micron scale [16]. The experiments consisted of probing the sample surface at different locations, with a needle of diameter ≈ 100 nm, in a hardened white cement paste. The indentation modulus M and the hardness H are measured directly for each location. By means of a self consistent analysis to associate the measured values of the indentation modulus M to the packing fraction ϕ_0 of a random assembly of spherical nano-scale grains, the experiments indicate that, within the same sample of C–S–H, such packing fraction varies significantly with location. Moreover, ϕ_0 ranges between 0.5 and 1, with values clustering between 0.6 and 0.8. M increases linearly with ϕ_0, as shown in Fig. 6, and extrapolates to zero at $\phi_0 \sim 0.5$.

In order to rationalize these experimental observations, we have considered that, in the hardened paste, the dense C–S–H gel can be well represented by a disordered assembly of colloidal hydrates. We produce disordered sub-micrometer structures using a Monte Carlo space filling algorithm that minimizes the interaction energy [45], where for the effective interactions between the colloidal particles we use a simple well potential as discussed in detail in Refs. [46]. The internal, sub-nanometric structure of C–S–H hydrates is known to be anisotropic, as it is characterized by silicate chains and calcium oxide layers with water layers in the interlaminar spaces between them [47–49]. For the moment, and for sake of simplicity, we assume that anisotropy is lost, on average, over distances of few nanometers, due to random orientation of the layers and spherical colloidal units are again a good approximation, leaving the shape anisotropy for future work. We consider that the hydrates get strongly bonded in the gel through the calcium-silicate layers and therefore the interaction strength must depend, among other factors, on the contact area between pairs of particles, viz. the size of the interface between them. We account for this by considering polydisperse particle size and a size dependent interaction strength. We have characterized the elastic properties of the model C–S–H structures in terms of the tensor of elasticity, computed keeping fixed the simulation box after equilibration to zero stress, and using the stress fluctuation method[50]. Increasing the degree of polydispersity leads to higher stiffnesses, due the higher packing fractions and different stress distribution

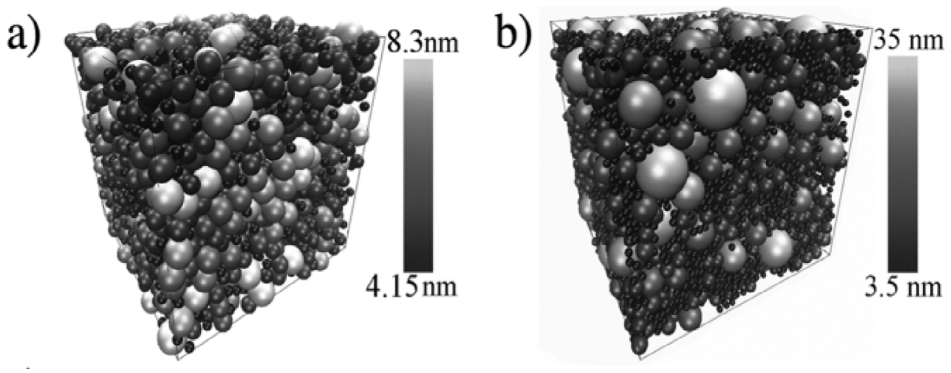

Fig. 7. Snapshots from simulations for C–S–H gel microstructures corresponding to different volume fractions, obtained with different size polydispersity. The color code indicates the particle size that in the model is indicative of the strength of cohesion.

attained. For an isotropic material, we can use the Voigt formulas to compute the bulk (K) and shear (G) moduli from the components of [C] and obtain the indentation modulus M [16,51] $M = 4G\frac{3K+G}{3K+4G}$. The results of numerical simulations from Ref. [46] are shown in Fig. 6: a good quantitative agreement with the experiments can be obtained only by considering a sufficiently high degree of polydispersity (up to 50%). Because of the assumptions made in our model, this finding indicates that the different values of the indentation modulus detected in the experiments should be related to a high degree of mechanical heterogeneities in the material. The higher local densities that lead to a higher modulus (as to be expected) are reached only thanks to the presence of a wide distribution of local densities and local mechanical strengths. As a result, the emerging picture is that in the hardened paste C–S–H must be characterized by the coexistence of relatively soft domains within stiffer regions and that such heterogeneities do affect the mechanical response of the material up to the sub-micrometric domains tested by nanoindentation.

In Fig. 7 we show two snapshots from the simulations, where the shade of grey allows us to distinguish the softer and stiffer domains. The findings obtained through this simple statistical physics approach have important consequences: the information on mechanical nano-scale heterogeneities whose effects extends nearly up to the micrometer scale are crucial for cement constitutive models and could be included in models aimed at elucidating the mechanical response detected at the micrometer scale [52]. The numerical simulations briefly reviewed here allowed us also to elucidate how the soft domains are significantly more liable to local rearrangements, while the strongly cohesive large particles constitute the high stiffness backbone of the microstructure [46]. Hence the size polydispersity or the mechanical heterogeneities apparently control the arising of irreversible structural rearrangements under deformation, which are good candidates as nano-scale mechanisms underlying mechanical aging and slow structural relaxation in the C–S–H gels. Nevertheless, we find that large particles behave as inclusions that hardly move and that need to be "excluded" by the rearrangement of the rest of the system in order for yielding to occur, suggesting that a high degree of size polydispersity or of mechanical heterogeneity may also eventually result in a broader elastic regime in the mechanical response of the material. Local densities, stiffness and size of the harder/softer domains could in principle be tuned via the chemical environment and the kinetics during the hydration process. The results just discussed therefore suggest a possible path to eventually change or even design the mechanics of the material.

4 Conclusions

In spite of its practical relevance to the material properties of concrete, the most used building material, the formation of calcium-silicate-hydrate gels during cement hydration is still poorly understood. The underlying physics entails considerable complexity and possibly shares several intriguing aspects with other soft materials in presence of thermodynamic gradients or out-of-equilibrium processing conditions. Here, we have briefly reviewed a few open questions that are related to technological developments and environmental sustainability. They all point to the necessity of deeper understanding of the fundamental physical mechanisms controlling the formation and the mechanics of the nano-scale C–S–H gel. We have given an overview of a few recent results obtained via statistical physics numerical simulations and new soft matter approaches for this problem. Using particle based statistical physics coarse-grained models, we were able to investigate the coupling between the gel morphology and the kinetics of the hydration process in the early stages of cement hydration and the role of mechanical heterogeneities in the hardened cement paste. The findings discussed here demonstrates how significant new insight can be obtained over lengthscales and phenomena that are observed in experiments and can be important for the technologically and environmentally relevant questions. These studies open the way to a new quantitative understanding of the physico-chemical complexity of this important material.

The authors acknowledge support from the Swiss National Science Foundation (SNSF) (Grants No. PP00P2_126483/1). The Concrete Sustainability Hub at MIT has supported this work with sponsorship provided by the Portland Cement Association (PCA) and the NRMCA Research and Education Foundation. E.M. F.J.U. and R.J.-M.P. wish to thank Schlumberger for partial support through the XCEM program. This work has been partly carried out within the framework of the ICoME2 Labex (ANR-11-LABX-0053) and the A*MIDEX projects (ANR-11-IDEX-0001-02) cofunded by the French program "Investissements d'Avenir", which is managed by the ANR, the French National Research Agency.

References

1. R.J.M. Pellenq, H. Van Damme, MRS Bull. **29**, 319 (2004)
2. R.J. Flatt, N. Roussel, C.R. Cheeseman, J. Eur. Ceram. Soc. **32**, 2787 (2012)
3. K. Van Vliet, R. Pellenq, M.J. Buehler, J.C. Grossman, H. Jennings, F.J. Ulm, S. Yip, MRS Bull. **37**, 395 (2012)
4. A. Nonat, Cem. Concr. Res. **34**, 1521 (2004)
5. A.J. Allen, J.J. Thomas, H.M. Jennings, Nature Mater. **6**, 311 (2007)
6. I. Richardson, Cem. Concr. Res. **38**, 137 (2008)
7. J.J. Thomas, H.M. Jennings, Cem. Concr. Res. **36**, 30 (2006)
8. W.S. Chiang, E. Fratini, P. Baglioni, D. Liu, S.H. Chen, J. Phys. Chem. C **116**, 5055 (2012)
9. F. Ridi, E. Fratini, P. Baglioni, J. Colloid Interface Sci. **357**, 255 (2011)
10. S. Garrault, E. Finot, E. Lesniewska, A. Nonat, Mater. Struct. **38**, 435 (2005)
11. J.W. Bullard, H.M. Jennings, R.A. Livingston, A. Nonat, G.W. Scherer, J.S. Schweitzer, K.L. Scrivener, J.J. Thomas, Cem. Concr. Res. **41**, 1208 (2011)
12. L.B. Skinner, S.R. Chae, C.J. Benmore, H.R. Wenk, P.J.M. Monteiro, Phys. Rev. Lett. **104**, 195502 (2010)
13. D. Bentz, Cement and Concrete Research **38**, 196 (2008), Special Issue The 12th International Congress on the Chemistry of Cement, Montreal, Canada, July 8–13, 2007
14. D. Lootens, P. Hébraud, E. Lécolier, H. Van Damme, Oil Gas Sci. Technol. **59**, 31 (2004)
15. L. Nachbaur, J. Mutin, A. Nonat, L. Choplin, Cem. Concr. Res. **31**, 183 (2001)

16. G. Constantinides, F.J. Ulm, J. Mech. Phys. Solids **55**, 64 (2007)
17. M. Vandamme, F.J. Ulm, Proc. Nat. Acad. Sci. **106**, 10552 (2009)
18. R.J.M. Pellenq, A. Kushima, R. Shahsavari, K.J. Van Vliet, M.J. Buehler, S. Yip, F.J. Ulm, Proc. Natl. Acad. Sci. USA **106**, 16102 (2009)
19. S. Bishnoi, K.L. Scrivener, Cem. Concr. Res. **39**, 266 (2009)
20. J.W. Bullard, E. Enjolras, W.L. George, S.G. Satterfield, J.E. Terrill, Mod. Sim. Mater. Sci. Eng. **18**, 025007 (2010)
21. F. Tzschichholz, H.J. Herrmann, H. Zanni, Phys. Rev. E **53**, 2629 (1996)
22. H.M. Jennings, Cem. Concr. Res. **30**, 101 (2000)
23. H.M. Jennings, Cem. Concr. Res. **38**, 275 (2008)
24. S. Brisard, R.S. Chae, I. Bihannic, L. Michot, P. Guttmann, J. Thieme, G. Schneider, P.J. Monteiro, P. Levitz, Am. Mineral. **97**, 480 (2012)
25. I. Richardson, Cem. Concr. Res. **34**, 1733 (2004)
26. E.M. Gartner, Cem. Concr. Res. **27**, 665 (1997)
27. E.M. Gartner, K.E. Kurtis, P.J.M. Monteiro, Cem. Concr. Res. **30**, 817 (2000)
28. A.C.A. Muller, K.L. Scrivener, A.M. Gajewicz, P.J. McDonald, J. Phys. Chem. C **117**, 403 (2013)
29. E. Gallucci, P. Mathur, K. Scrivener, Cem. Concr. Res. **40**, 4 (2010)
30. S. Bishnoi, Cem. Concr. Res. **46**, 30 (2013)
31. K. Ioannidou, R.J.M. Pellenq, E. Del Gado, Soft Matter **10**, 1121 (2014)
32. S. Garrault, T. Behr, A. Nonat, J. Phys. Chem. B **110**, 270 (2006), ISSN 1520-6106
33. E. Masoero, J.J. Thomas, H.M. Jennings, J. Am. Ceram. Soc. (2013) (in press)
34. R.J.M. Pellenq, J.M. Caillol, A. Delville, J. Phys. Chem. B **101**, 8584 (1997)
35. B. Jönsson, A. Nonat, C. Labbez, B. Cabane, H. Wennerström, Langmuir **21**, 9211 (2005)
36. R.M. Pellenq, N. Lequeux, H. van Damme, Cem. Concr. Res. **38**, 159 (2008)
37. Y.S. Jho, R. Brewster, S.A. Safran, P.A. Pincus, Langmuir **27**, 4439 (2011)
38. C. Plassard, E. Lesniewska, I. Pochard, A. Nonat, Langmuir **21**, 7263 (2005)
39. S. Lesko, E. Lesniewska, A. Nonat, J.C. Mutin, J.P. Goudonnet, Ultramicroscopy **86**, 11 (2001)
40. M.J. Booth, A.C. Eaton, A.D.J. Haymet, J. Chem. Phys. **103**, 417 (1995)
41. P. Attard, *Electrolytes and the Electric Double Layer* (John Wiley & Sons, Inc., 2007), p. 1
42. A. de Candia, E. Del Gado, A. Fierro, N. Sator, M. Tarzia, A. Coniglio, Phys. Rev. E **74**, 010403 (2006)
43. P. Charbonneau, D.R. Reichman, Phys. Rev. E **75**, 011507 (2007)
44. L. Nicoleau, T. Gadt, L. Chitu, G. Maier, O. Paris, Soft Matter **9**, 4864 (2013)
45. E. Masoero, E. Del Gado, R.J.M. Pellenq, F.J. Ulm, S. Yip, Phys. Rev. Lett. **109**, 155503 (2012)
46. E. Masoero, E. Del Gado, R.J.M. Pellenq, S. Yip, F.J. Ulm, Soft Matter. **10**, 491 (2014)
47. H. Taylor, Adv. Cem. Based Mater. **1**, 38 (1993)
48. X. Cong, R.J. Kirkpatrick, Adv. Cem. Based Mater. **3**, 144 (1996)
49. I. Richardson, Cem. Concr. Res. **29**, 1131 (1999)
50. J.F. Lutsko, J. Appl. Phys. **65**, (1989)
51. J.F. Nye, *Physical Properties of Crystals: Their Representation by Tensors and Matrices* (Oxford University Press, 1985)
52. G.W. Scherer, J. Zhang, J.A. Quintanilla, S. Torquato, Cem. Concr. Res. **42**, 665 (2012)